Resonant microwaves probing the spatial afterglow of an RF plasma jet

Resonant microwaves probing the spatial afterglow of an RF plasma jet

Cite as: Appl. Phys. Lett. **115**, 254103 (2019); https://doi.org/10.1063/1.5127744
Submitted: 12 September 2019 . Accepted: 07 December 2019 . Published Online: 18 December 2019

B. Platier, T. J. A. Staps, M. van der Schans, W. L. IJzerman, and J. Beckers

Applied Physics Letters ARTICLE scitation.org/journal/apl

Resonant microwaves probing the spatial afterglow of an RF plasma jet

Cite as: Appl. Phys. Lett. **115**, 254103 (2019); doi: 10.1063/1.5127744
Submitted: 12 September 2019 · Accepted: 7 December 2019 ·
Published Online: 18 December 2019

View Online Export Citation CrossMark

B. Platier,[1,a] T. J. A. Staps,[1] M. van der Schans,[1,2] W. L. IJzerman,[2,3] and J. Beckers[1]

AFFILIATIONS

[1]Department of Applied Physics, Eindhoven University of Technology, PO Box 513, 5600MB Eindhoven, The Netherlands
[2]Signify, High Tech Campus 7, 5656AE Eindhoven, The Netherlands
[3]Department of Mathematics and Computer Science, Eindhoven University of Technology, PO Box 513, 5600MB Eindhoven, The Netherlands

[a)]b.platier@tue.nl

ABSTRACT

The electron density and effective electron collision frequency in the spatial afterglow of a pulsed radio frequency driven atmospheric-pressure plasma jet are obtained by using microwave cavity resonance spectroscopy in a temporal manner with an ∼1 μs resolution. During the "plasma on" phase, values of $1.7 \pm 0.3 \times 10^{18}$ m^{-3} for the electron density and 0.12 ± 0.01 THz for the electron collision frequency were found. These values and standard deviations represent the collective measurement set with repetition rates ranging from 125 to 8000 Hz. The spread in the plasma parameters during this phase within one repetition frequency is smaller than 3%. It is observed that remnant species, e.g., metastables, of previous discharges influence the decay of the plasma. The work reported is enabled by recent developments in the applied diagnostic with respect to the resolution in the plasmas' permittivity. Moreover, a multiplying probe is used for the electrical characterization of the plasma and the presence of the cavity did not influence the plasma impedance. This strongly suggests that the cavity did not affect the discharge.

Radio-frequency (RF) driven atmospheric-pressure plasma jets are extremely important "tools" for numerous industrial processes such as plasma-assisted cleaning and coating,[1] deposition,[2] and sterilization.[3] Furthermore, these sources show high potential in plasma medicine[4] with respect to wound healing[5] and cancer treatment.[6] The combination of low gas temperatures, high concentrations of reactive species, and no need for expensive vacuum systems is a major advantage of RF jets over conventional plasma sources.[7]

The electron density n_e is one of the most important plasma parameters, and accurately diagnosing the electron dynamics is key to further develop and optimize the aforementioned applications. Until now, several electron diagnostics have been used in experiments. For instance, the broadening of spectral emission lines can be used to determine n_e.[8] The application of this principle, however, is restricted to only those regions where plasma emission is of sufficient intensity. Another strong diagnostic, Thomson scattering—based on the scattering of laser light by free electrons—has been applied to measure the electron density in atmospheric pressure radio frequency and microwave driven plasmas.[9–11] Although the temporal and spatial resolutions are high, the lower detection limit of it is around 10^{18} m^{-3}.[9] In most applications of RF plasma jets, the interaction of the plasma with the treated target takes place downstream from the position where the plasma is generated. Specifically, from the so-called spatial plasma afterglow region, light emission is too faint to retrieve information about the free electrons from optical emission spectroscopy measurements. At the same time, in this spatial afterglow region, electron densities are expected at or below the detection limit of Thomson scattering.

This Letter introduces the application of microwave cavity resonance spectroscopy (MCRS) to monitor *in situ* the electron dynamics temporally resolved with an ∼1 μs time resolution in this highly interesting afterglow region.

Since the development of MCRS in the 1940s,[12] it has been used to study various types of low-pressure plasmas: pristine RF driven plasmas,[13,14] etching plasmas,[15] powder-forming plasmas,[16–18] and EUV photon-induced plasmas.[19,20] In all these works, the plasma-induced change in resonant behavior of a standing wave in a cavity—a void enclosed by conductive walls—due to a change in permittivity of the medium inside the cavity is used to determine plasma parameters.

Only recently, van der Schans *et al.*[21] extended the operational range of MCRS by demonstrating that MCRS can be used on atmospheric-pressure plasmas as well to determine the electron density and effective electron collision frequency between successive discharges in a high voltage pulsed plasma jet in N_2 feed gas. Moreover, the resolution of the diagnostic has been improved in recent publications.[20,21]

In this work, MCRS is applied to an RF driven plasma jet and, more specifically, to the spatial afterglow of such a jet. The spatial afterglow region where electrons have thermalized to values close to room temperature due to multiple collisions with the background gas is investigated to demonstrate the renewed capabilities—in resolution and operating range—of the diagnostic method. In contrast to our earlier work where only the decay of the plasma could be investigated,[21] here the formation, the steady state, and the decay phases are studied. Furthermore, the method is enhanced by compensation for thermal expansion of the cavity, while the resolution in the real part of the permittivity is increased by again one order of magnitude.

The main components of the experimental setup were the plasma source and the microwave resonance cavity including the control and readout electronics. A schematic overview of the experimental setup is shown in Fig. 1, while a more detailed view of the discharge geometry can be found in Fig. 2.

The atmospheric pressure discharges were generated with an excitation frequency of 13.56 MHz in He working gas (purity of 99.999%) flowing at a volumetric rate of 1 slm into surrounding air. A function generator, an RF amplifier, and a tunable coil for impedance

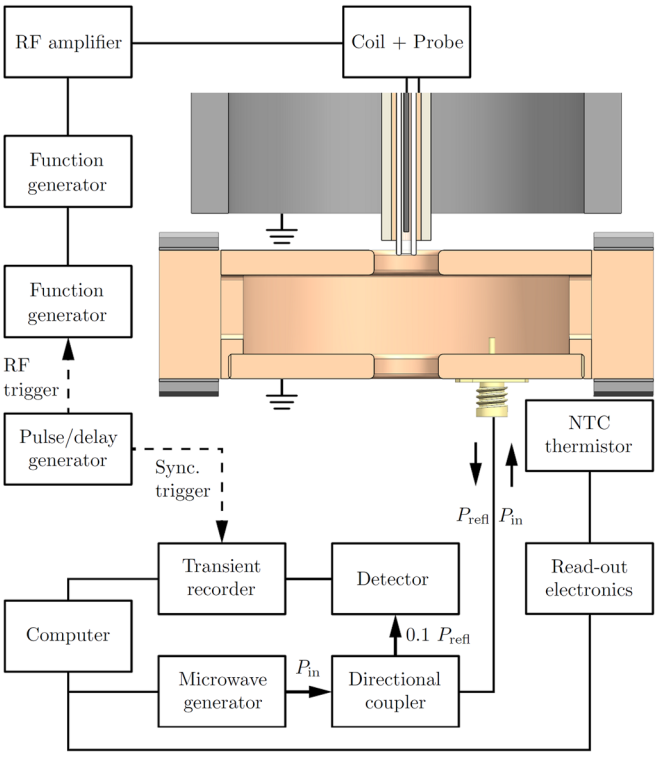

FIG. 1. A schematic overview of the experimental setup consisting of the plasma source and cavity including the control and readout electronics.

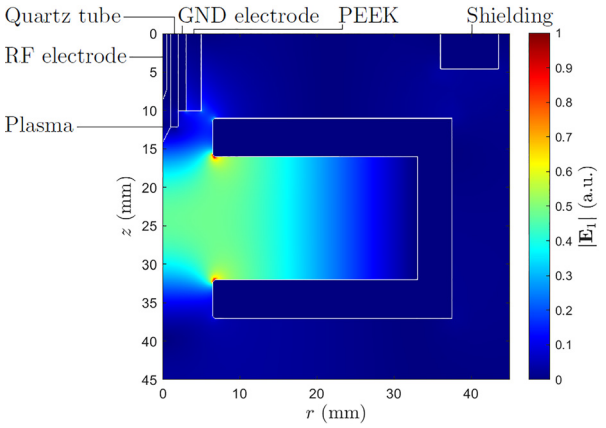

FIG. 2. A schematic of the plasma source geometry and the resonance cavity with the electric field magnitude of the TM_{010} mode.

matching were used to generate the plasma. The function generator was amplitude modulated by a second function generator that was gated by a pulse/delay generator in order to generate pulsed plasma discharges with a temporal width of 50 μs at a repetition rate f_{rep} to be set between 125 and 8000 Hz. With these settings, the duty cycle was varied from 40% to 0.625%. The RF voltage was applied to an electrode that had a radius of 0.5 mm and a tip angle of approximately 40°. This needle electrode was placed concentrically inside a quartz tube of inner radius 1 mm and outer radius 2 mm, with the end of the pin located 3.5 mm before the end of the quartz tube. The cylindrical shell shaped grounded electrode was placed around and in contact with the dielectric. The parasitic capacitance of the plasma source was predefined by shielding the electrodes.

For the electrical characterization of the plasma, i.e., measurement of the driving voltage, current, and power, a multiplying probe—which was insensitive to changes in the load impedance—as described in Ref. 22 was further developed and incorporated in the plasma source. The temporal resolution of the power was limited by an electronic filter to 30 μs. An oscilloscope was used to monitor the outputs of the probe. This probe was used to investigate the influence of the cavity on the plasma. No change in the load impedance was observed, which strongly suggests that the discharge is unaffected by the presence of the cavity.

As the MCRS diagnostic and method are already described in several other works,[20,21] describing only the key features suffices here. The resonant behavior of a standing wave in a cavity is described by the spectral position of the resonance peak f_{res} and the full-width-at-half-maximum (FWHM) of the peak Γ, which is indicated by the quality factor Q given by $Q = f_{\mathrm{res}}/\Gamma$.

Assuming a uniform plasma volume and following the approach of van der Schans *et al.*,[21] the change in relative resonance frequency $\Delta f/f_1$ and reciprocal quality factor $\Delta(1/Q)$ are the parameters to be measured and used to determine the effective collision frequency ν_{eff},

$$\nu_{\mathrm{eff}} = \pi f_1 \frac{\Delta(1/Q)}{\Delta f/f_1}, \tag{1}$$

and the electron density n_e,

$$n_e = 2\frac{\varepsilon_0 m_e}{e^2}\frac{\nu_{eff}^2 + 4\pi^2 f_1^2}{\mathcal{V}}\frac{\Delta f}{f_1}, \quad (2)$$

where ε_0 is the vacuum permittivity, m_e the mass of an electron, e the elementary charge, and f_1 the resonance frequency of the empty cavity. $\mathcal{V}$ is the ratio of the effective (microwave-field-squared-weighted) plasma volume and the effective (microwave-field-squared-weighted) cavity volume given by

$$\mathcal{V} = \frac{\iiint_{V_p} |\mathbf{E}_1|^2 d^3\mathbf{r}}{\iiint_{V_{cav}} |\mathbf{E}_1|^2 d^3\mathbf{r}}, \quad (3)$$

where V_{cav} and V_p are the occupied volume of the cavity and plasma, respectively.

A cylindrical copper microwave cavity with an inner radius of 33 mm, a height of 16 mm, and a resonance frequency f_{res} of 3.5 GHz for the TM_{010} mode was used. This mode had a quality factor of $Q = 4 \times 10^3$ and therefore provided a temporal resolution of $\sim$1 μs. The parts of the cavity were vacuum soldered together, resulting in a very high mechanical stability that translated into excellent reproducibility compared to the aforementioned works. Concentric holes of 13 mm in diameter in the top and bottom flat walls allowed the gas flow and discharge to enter and exit the cavity. Note that at the position, i.e., the cavity axis, where the plasma afterglow entered the cavity volume, the electric field of the mode was the highest, resulting in the highest MCRS signal per free electron. The quartz tube of the plasma source protruded the top hole by 1 mm, which had no significant influence on the resonant behavior of the cavity as a whole.

A microwave signal with frequency $f = \omega/2\pi$ and power P_{in} (1 mW) was generated by a microwave generator. These microwaves traveled through a directional coupler and were applied to a straight antenna that protruded a few mm into the cavity. Reflected microwaves returned to the directional coupler where 10% of the power was directed to a logarithmic power detector. The reflected power P_{refl} depended on the applied frequency as the cavity was only able to absorb power when the applied frequency matches a resonance frequency. The temporal response of the power detector was sampled at 10 MHz using a transient recorder, which was triggered by the same pulse/delay generator to synchronize the measurements with the discharges. Allowed by the extremely high reproducibility of the discharge dynamics, multiple discharges were used to create a spectral response for each time step and to reduce noise by averaging. Computer code was used to set the applied frequency and save the data of the transient recorder. In this work, 256 discharges were used to determine the temporal response of the cavity at each frequency. Frequencies ranging from 3.509 to 3.516 GHz with intervals of 5 kHz were probed.

For each set of discharges with the same f, the temperature of the cavity T_{cav} was logged with submilliKelvin resolution by an NTC thermistor in combination with in-house developed readout electronics. This high resolution was needed to compensate for the apparent frequency shift due to thermal expansion of the cavity caused by fluctuations in the lab temperature of $\sim$1 K.

In contrast to most MCRS measurements on low-pressure plasmas, in the experiment presented here, the plasma only filled a fraction of the cavity and therefore $\mathcal{V} \ll$ unity. In order to determine the effective plasma volume ratio, the resonant field profile and the plasma volume were required. The electric field profile of the TM_{010} mode for the empty cavity $|\mathbf{E}_1|$ was calculated with the frequency domain electromagnetic wave toolbox in COMSOL[23] and is presented in Fig. 2. V_p was determined by imaging the light-emitting volume with a camera with a macrozoom lens. From the simulated electric field profile and the camera images, it was estimated that $\mathcal{V} \approx 1.7 \times 10^{-6}$. The level of accuracy of this estimation is the order of its magnitude, which in its turn limits the accuracy of the electron densities presented below.

The camera images show that the light-emitting volume of the plasma extends to 2 mm outside the quartz tube. At atmospheric pressure, the energy relaxation length[24] is $<$50 μm for electrons with $\leq$10 eV kinetic energy to cool down to room temperature. As the probed region here is relatively far away from the RF electrode and partially outside the glass tube, the electrons are expected to be near room temperature and gas mixing, i.e., mixing with surrounding air, is likely to occur.

For the repetition rates of 125, 500, 2000, and 8000 Hz, $\Delta f/f_1$ and $\Delta(1/Q)$, and from these, derived values of n_e and ν_{eff} as a function of time are shown in Figs. 3(a)–3(d). In this time frame, the plasma was ignited at $t = 50$ μs and the RF power was provided for a duration of 50 μs. Four consecutive plasma dynamical phases can be identified, which are indicated in the figures by Roman numerals and will be described individually hereafter.

Phase I is used to determine f_1 and Q_1 for the "empty" cavity. Figures 3(a) and 3(b) show clearly that the response for $f_{rep} = 8000$ Hz was still converging during these 10 μs before ignition of the next plasma event. This leads to an error in the results for this repetition rate. From the response of the other repetition rates, it can be seen that the noise level in the resonance frequency is decreased by one order of magnitude with respect to our previous publication[21] to a standard deviation of 1-σ $<$ 25 Hz.

In phase II, the plasma is formed and an increase in electron density and the effective collision frequency is observed over roughly 20 μs.

In phase III, the plasma power measured by the multiplying probe converges at 20.0 $\pm$ 0.2 W. Nevertheless, it can be assumed that this is the power during the whole phase as the steady state is reached. The standard deviations of the plasma parameters within one f_{rep} are smaller than 3%. For all f_{rep} combined, the found n_e and ν_{eff} are $1.7 \pm 0.3 \times 10^{18}$ m^{-3} and 0.12 $\pm$ 0.01 THz, respectively. Following the approach reported in Ref. 25, near the electrode, n_e is estimated as 5×10^{18} m^{-3} and the typical length over which electrons can diffuse is $\sim$1 mm. As this length is comparable with the size of the plasma, the estimation of n_e is also valid for the probed region for which very similar densities were found experimentally. ν_{eff}, unlike n_e, is unaffected by the systematic error arising from the effective volume. The value of ν_{eff} is close to 0.15 THz, which was calculated from the effective electron-neutral collision cross sections[26] for atmospheric-pressure He and electrons at room temperature. The small difference in the experimental and theoretical value can be attributed to in-mixing, as similar calculations provided ν_{eff} for N_2 and O_2 of 0.08 and 0.03 THz, respectively. This approach might be an elegant way to measure the composition of the background gas in future experiments.

In phase IV, after turning off the RF power, n_e and ν_{eff} decrease as can be seen in Fig. 3(e). Approximately 200 ns later, a brief increase in the electron density is observed. As described earlier in the literature,[27] this effect can most likely be attributed to Penning ionization. Δn_e, i.e., the difference between n_e at the end of the previous phase ($t = 100$ μs) and the maximum in phase IV, is indicated in Fig. 3(f) for

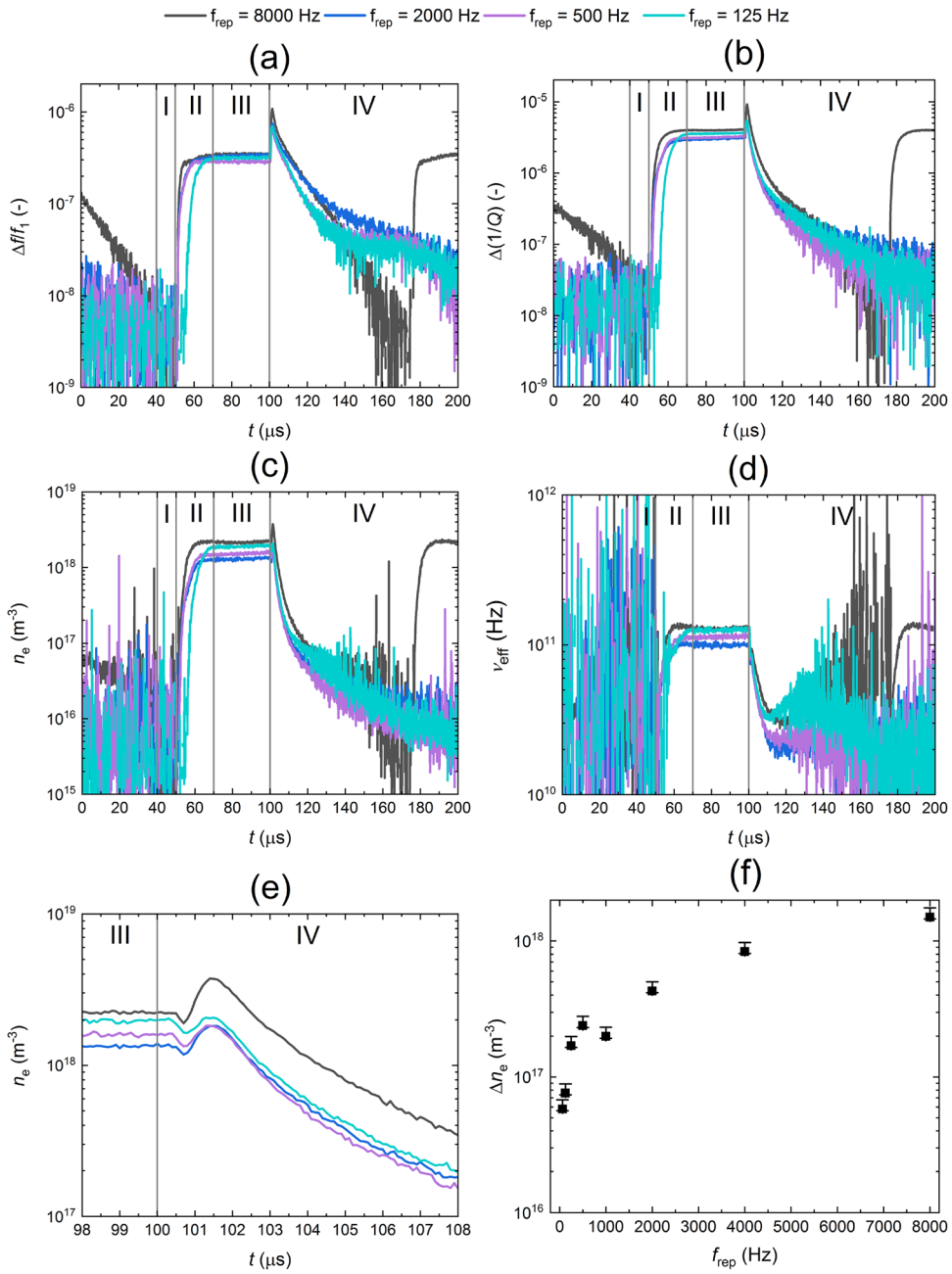

FIG. 3. Temporal evolution of (a) the relative frequency shift, (b) the change of the reciprocal quality factor, (c) the electron density, (d) the effective electron collision frequency for different plasma repetition frequencies, and (e) the electron density around the moment of turning off the RF power. The difference in electron density between $t = 100$ μs and in the peak as a function of the repetition frequency is shown in (f). The Roman numerals indicate the four phases in the experiment.

several values of f_{rep}. The error in Δn_e is dominated by a term, which relates to the fact that the cavity was not fast enough to follow the changes in the plasma at this moment in the evolution. A trend in the number of additionally created electrons is observed: Δn_e increases while decreasing the time between the RF pulses. This can be attributed to, e.g., the less decay of remnant species of previous discharges or a change in reaction rates due to gas heating.

After this brief increase in n_e, the decay of the electron density and the effective collision frequency continues. At $t = 175$ μs, the start of the successive discharge for a repetition rate of 8000 Hz can be seen in Figs. 3(a)–3(d).

The obtained temporal evolution from $t \approx 120$ μs onward would have been below the noise level without the advancements developed in this work. The improved mechanical stability and higher Q of the

cavity and the increased number of responses used in the analysis resulted in 1-σ in the real part of the relative permittivity of 1×10^{-8}. The lowest value of the electron density that can be detected depends on ν_{eff} and $\mathcal{V}$. If the collisions can be neglected and the plasma fills the whole cavity, the lower-detection limit is $\sim 2 \times 10^{9}$ m^{-3}. For $\nu_{\text{eff}} = 1$ THz and $f_{\text{res}} = 3.5$ GHz, this limit is $\sim 4 \times 10^{12}$ m^{-3} when the whole cavity is filled and $\sim 2 \times 10^{18}$ m^{-3} for $\mathcal{V} = 1.7 \times 10^{-6}$. During phase III, the resolution in n_e is $\sim 3 \times 10^{16}$ m^{-3}, which is 2% of the measured value. When the changes in resonant behavior are very small with respect to the empty cavity, the properties of the electrons can no longer be assumed to be the only contributors to changes in permittivity. This opens up a playground for exploring other (plasma-induced) phenomena affecting the permittivity.

In conclusion, this work demonstrates that microwave cavity resonance spectroscopy is capable of resolving the electron dynamics during all phases of the evolution of the spatial afterglow of a pulsed radio frequency driven atmospheric-pressure plasma jet. Furthermore, no changes in the electrical characteristics of the plasma due to the presence of the cavity were observed, which strongly suggests that the cavity did not affect the discharge.

The authors are grateful to Paul Beijer for developing the multiplying probe and Ieman Koole for inventing the apparatus used for the temperature measurements.

REFERENCES

[1]R. Foest, E. Kindel, H. Lange, A. Ohl, M. Stieber, and K. D. Weltmann, Contrib. Plasma Phys. **47**, 119 (2007).
[2]O. V. Penkov, M. Khadem, W. S. Lim, and D. E. Kim, J. Coat. Technol. Res. **12**, 225 (2015).
[3]R. Brandenburg, J. Ehlbeck, M. Stieber, T. V. Woedtke, J. Zeymer, O. Schlüter, and K. D. Weltmann, Contrib. Plasma Phys. **47**, 72 (2007).
[4]M. G. Kong, G. Kroesen, G. Morfill, T. Nosenko, T. Shimizu, J. Van Dijk, and J. L. Zimmermann, New J. Phys. **11**, 115012 (2009).
[5]J. Winter, R. Brandenburg, and K.-D. Weltmann, Plasma Sources Sci. Technol. **24**, 064001 (2015).
[6]M. Keidar, D. Yan, I. I. Beilis, B. Trink, and J. H. Sherman, Trends Biotechnol. **36**, 586 (2018).
[7]A. Schütze, J. Y. Jeong, S. E. Babayan, J. Park, G. S. Selwyn, and R. F. Hicks, IEEE Trans. Plasma Sci. **26**, 1685 (1998).
[8]A. Y. Nikiforov, C. Leys, M. A. Gonzalez, and J. L. Walsh, Plasma Sources Sci. Technol. **24**, 034001 (2015).
[9]A. F. H. Van Gessel, E. A. D. Carbone, P. J. Bruggeman, and J. J. A. M. Van Der Mullen, Plasma Sources Sci. Technol. **21**, 015003 (2012).
[10]B. Van Gessel, R. Brandenburg, and P. Bruggeman, Appl. Phys. Lett. **103**, 064103 (2013).
[11]S. Hübner, J. S. Sousa, J. Van Der Mullen, and W. G. Graham, Plasma Sources Sci. Technol. **24**, 054005 (2015).
[12]M. A. Biondi and S. C. Brown, Phys. Rev. **75**, 1700 (1949).
[13]J. Franek, S. Nogami, M. Koepke, V. Demidov, and E. Barnat, Plasma **2**, 65 (2019).
[14]J. Faltýnek, V. Kudrle, J. Tesař, M. Volfová, and A. Tálský, Plasma Sources Sci. Technol. **28**, 105007 (2019).
[15]E. Stoffels, W. W. Stoffels, D. Vender, M. Kando, G. M. Kroesen, and F. J. De Hoog, Phys. Rev. E **51**, 2425 (1995).
[16]J. Beckers, W. W. Stoffels, and G. M. W. Kroesen, J. Phys. D: Appl. Phys. **42**, 155206 (2009).
[17]G. Wattieaux, N. Carrasco, M. Henault, L. Boufendi, and G. Cernogora, Plasma Sources Sci. Technol. **24**, 015028 (2015).
[18]G. Alcouffe, M. Cavarroc, G. Cernogora, F. Ouni, A. Jolly, L. Boufendi, and C. Szopa, Plasma Sources Sci. Technol. **19**, 015008 (2010).
[19]R. M. Van Der Horst, J. Beckers, S. Nijdam, and G. M. W. Kroesen, J. Phys. D: Appl. Phys. **47**, 302001 (2014).
[20]J. Beckers, F. M. Van De Wetering, B. Platier, M. A. Van Ninhuijs, G. J. Brussaard, V. Y. Banine, and O. J. Luiten, J. Phys. D: Appl. Phys. **52**, 034004 (2019).
[21]M. van der Schans, B. Platier, P. Koelman, F. van de Wetering, J. Van Dijk, J. Beckers, S. Nijdam, and W. IJzerman, Plasma Sources Sci. Technol. **28**, 035020 (2019).
[22]P. A. Beijer, A. Sobota, E. M. Van Veldhuizen, and G. M. Kroesen, J. Phys. D: Appl. Phys. **49**, 104001 (2016).
[23]See https://www.comsol.com/rf-module for "COMSOL, Modeling Software for RF, Microwave, and Millimeter-Wave Designs," (last accessed August 26, 2019).
[24]M. S. Benilov, J. Phys. D: Appl. Phys. **33**, 1683 (2000).
[25]S. Hofmann, A. F. Van Gessel, T. Verreycken, and P. Bruggeman, Plasma Sources Sci. Technol. **20**, 065010 (2011).
[26]See www.lxcat.net, for "Phelps database" (last accessed on August 5, 2019).
[27]R. Deloche, P. Monchicourt, M. Cheret, and F. Lambert, Phys. Rev. A **13**, 1140 (1976).